Polymer 51 (2010) 2040–2048

Contents lists available at ScienceDirect

Polymer

journal homepage: www.elsevier.com/locate/polymer

Filler/matrix-debonding and micro-mechanisms of deformation in particulate filled polypropylene composites under tension

Michael Jerabek [a,*], Zoltan Major [b], Károly Renner [c,d], János Móczó [c,d], Béla Pukánszky [c,d], Reinhold W. Lang [b]

[a] Polymer Competence Center Leoben GmbH, Rosegger Strasse 12, 8700 Leoben, Austria
[b] Institute of Materials Science and Testing of Plastics, University of Leoben, Franz-Josef-Strasse 18, 8700 Leoben, Austria
[c] Laboratory of Plastics and Rubber Technology, Department of Physical Chemistry and Materials Science, Budapest University of Technology and Economics, H-1521 Budapest, P.O. Box 92, Hungary
[d] Institute of Materials and Environmental Chemistry, Chemical Research Center, Hungarian Academy of Sciences, H-1525 Budapest, P. O. Box 17, Hungary

ARTICLE INFO

Article history:
Received 6 April 2009
Received in revised form
18 February 2010
Accepted 19 February 2010
Available online 26 February 2010

Keywords:
Particulate filled polypropylene
Micro-mechanisms of deformation
Volume strain

ABSTRACT

Volume strain measurements of particulate filled polypropylene (PP) composites containing different glass beads and talc as filler were carried out in tension as a function of temperature and strain rate to determine the micro-mechanisms of deformation. While local cavitation mechanisms (micro-voiding, crazing, and micro-cracking) and subsequent debonding of the particles dominated as failure mechanisms at high strain rates and at room temperature, a more significant contribution of local shear yielding was observed with a reduced contribution of cavitational mechanisms at low strain rates or at 80 °C. This change in the dominating micro-mechanisms of deformation resulted in smaller volume strains during the tensile loading of the composites than for the respective neat matrix. Moreover, a novel approach is introduced for the detection of debonding using volume strain measurements, which takes into account the dilatational and deviatoric behavior of the neat matrix polymer and the composite. The results are supported by acoustic emission measurements carried out simultaneously on the same specimens.

1. Introduction

Particulate filled polymer composites have been used in increasing quantities in various applications, e.g., in the automotive industry, for appliances or as garden furniture [1,2]. The properties of these composites are basically determined by the behavior of the matrix, the properties of the filler, the composition, the particle spatial distribution and the interfacial interaction [3]. Although such heterogeneous systems are of large scientific and practical interest, their behavior under external load is not fully understood. Further research is necessary to understand and to predict properly the debonding of the particles, i.e., the failure at the interface and the detachment of the particles from the matrix, as well as other micro-mechanisms of failure including shear yielding, crazing and micro-cracking.

The debonding stress is one of the key parameters of particulate filled composites and it is strongly related to particle size. Two models have been proposed in the literature [4–6] to calculate the debonding stress of spherical particles, which are not bonded chemically to the matrix. The first model derived by Vollenberg et al. [4,5] is based on the assumption that the mechanically stored potential energy around a spherical inclusion is used for the creation of new surfaces at the moment of debonding. The authors assumed that debonding takes place around the poles of the spherical particle and proceeds instantaneously at an angle of 25°. The second model developed by Pukánszky and Vörös [6] is also based on energy equalities but without the assumptions made by Vollenberg et al. [4,5] and gives the debonding stress, σ_D, as

$$\sigma_D = -C_1\sigma_T + C_2\left(\frac{W_{AB}E}{R}\right)^{\frac{1}{2}} \quad (1)$$

where C_1 and C_2 are constants having exact physical meanings, σ_T is the thermal stress induced by the different thermal expansion of the components, W_{AB} is the reversible work of adhesion, E is the tensile modulus of the matrix and R is the radius of the particles.

* Corresponding author. Present address. Borealis Polyolefine GmbH, St. Peter Strasse 25, 4021 Linz, Austria. Tel.: +43 732 6981 5744; fax: +43 732 6981 5910.
E-mail address: michael.jerabek@borealisgroup.com (M. Jerabek).

0032-3861/$ – see front matter © 2010 Elsevier Ltd. All rights reserved.
doi:10.1016/j.polymer.2010.02.033

Accordingly, smaller particles debond at higher stresses moreover, debonding occurs over a broad strain range due to the inherently wide particle size distribution of commercial fillers. The prediction of debonding stress is difficult with either model since their constants are not known and cannot be determined by simple measurements.

In order to detect the onset and to investigate the further progress of debonding, several methods have been proposed in the literature and applied in practice like in-situ tensile experiments [7], volume strain measurements [8–10] or the measurement of acoustic emission [11,12]. One of the first studies aimed at the determination of debonding stress of stiff particles in polymer composites was carried out by Vollenberg [4], who performed tensile tests under light microscope and assigned the initiation of the debonding process to a "kink" in the stress-strain curve. Since this irregularity in the stress-strain curve was not confirmed in later experiments, volume strain measurements have been used more and more frequently. Different approaches exist in the literature for the determination of the initiation of debonding. A bilinear fitting was applied to the volume strain curve and the intersection of these linear regimes was related to the onset of debonding in one approach [13], which, however, completely neglects the differences in the dilatational and deviatoric responses of the matrix and the composite, respectively. Another approach defines the onset of debonding as the deviation of the dilatational from the overall volume strain [9]. The behavior of the matrix is not considered in this approach, but the results showed that the matrix might deviate from the dilatational behavior of the composites at small strains. In order to account for the dilatational deformation of the matrix, Sinien et al. [14] proposed to subtract the volume strain of the matrix from that of the composite. They justified their approach with the help of high-precision volume strain measurements, but this method fails to predict the onset of debonding properly due to differences in Poisson's ratio and thus in the dilatational volume strain of the matrix and composite, respectively. To overcome the drawbacks of the approaches described above, Meddad and Fisa [8] suggested the subtraction of both the dilatational volume strain of the composite and the volume strain of the matrix from composite volume strain. The different local strain states (i.e., strain distribution and degree of constraint) in the matrix and in the composite are not considered in this procedure, so that this may lead to a significant error in the evaluation of the debonding stress. A model separating the dilatational, deviatoric and cavitational parts of the volume strain curve was developed by Heikens et al. [15], which may in principle also lead to reasonable results for the debonding stress in polymer composites deforming with a single, well defined mechanism. However, it must be emphasized that in filled polymer systems such as the particulate filled PP composites investigated in this study, several micro-mechanisms may contribute to an increase in the cavitational component of deformation (volume strain). This includes debonding at the particle-matrix interface, and various mechanisms of void formation, crazing, and micro-cracking in the matrix [16,17]. This, of course, complicates the experimental determination of the debonding stress via volume strain measurements.

In order to overcome the problems mentioned above and to make use of volume strain measurements for the characterization of the debonding process, a novel approach is introduced which is supported and verified by acoustic emission measurements. Hence, volume strain curves of the neat polymer, as well as talc and glass bead filled PP composites were determined and analyzed as a function of strain rate and temperature, and the dominating micromechanical deformation processes under various conditions were deduced.

Table 1
Nomenclature and composition of the materials investigated.

Material	Filler	Weight fraction of filler	Volume fraction of filler
PP	–	–	–
PP-G3.5S	GB-S	0.10	0.034
PP-G7.0S	GB-S	0.20	0.073
PP-G3.5L	GB-L	0.10	0.034
PP-G7.0L	GB-L	0.20	0.073
PP-T3.5	talc	0.09	0.035
PP-T7.0	talc	0.18	0.075

2. Experimental

2.1. Materials

The matrix material was a development grade PP homopolymer, provided by Borealis Polyolefine GmbH Linz (Linz, Austria) and delivered as injection molded tensile bars corresponding to ISO 3167 type B. The same material was extensively characterized in long-term compressive relaxation tests [18]. Two glass beads (GB) with different sizes, Spheriglass 3000 (GB-L), large, and Spheriglass 5000 (GB-S), small, from Potters Europe (Barnsley, UK), were used as spherical fillers. Luzenac A7 talc provided by Luzenac Europe (Toulouse, France) was used as non-spherical filler in order to change particle shape. Glass beads and talc were added at two different volume fractions to PP in order to study the influence of particle content on the deformation behavior of the composites. An overview of the nomenclature and composition of the composites studied is given in Table 1.

The mean particle size in number was determined from scanning electron micrographs (SEM) by counting more than 1000 particles for each of the fillers, as only particle size distributions in weight are available from the supplier. For an in-depth analysis of the various micro-mechanisms of deformation, information on particle size distributions in number are important and needed for representative micromechanical modeling and simulation. Due to the platy structure of talc, its aspect ratio was also determined by measuring the length and thickness of the platelets. Properties necessary for the understanding of the behavior of the composites are listed in Table 2.

2.2. Experimental setup

Tensile tests were performed using an electromechanical universal testing machine Instron 5500 (Instron LTD, High Wycombe, USA) at constant crosshead displacement rates of 0.01 mm/s and 1 mm/s corresponding to strain rates of $8.7 \times 10^{-5}\ s^{-1}$ and $8.7 \times 10^{-3}\ s^{-1}$. Tests were performed at 23 °C and 80 °C. Initial gauge length was 115 mm. The 3D Digital Image Correlation (DIC) system Aramis (Gesellschaft für optische Messtechnik mbH, Braunschweig, D) was utilized for the accurate

Table 2
Elastic properties and particle characteristics of the investigated fillers. Tensile modulus and Poisson's ratio were taken from the data sheets of the supplier.

Particle	Tensile modulus (GPa)	Poisson's ratio	Mean diameter (μm)	Specific surface area (m^2/g)	Aspect ratio	Coating
GB-S	70	0.21	1.31	1.0[b]	1	Yes
GB-L	70	0.21	1.58	0.6[b]	1	Yes
Talc	90[a]	0.21[a]	1.73	9.0[c]	8	No

[a] Determined on bulk material.
[b] Cisal test method.
[c] Determined by BET measurement.

determination of volume strain. The equipment is described in detail in Ref. [19]. To allow for a sufficient optical signal detection and to avoid heating of the specimen during testing, the light directed onto the specimen was provided by the cold light system Dedocool (Dedo Weigert Film GmbH; Munich, D).The 3D-DIC system consists of two cameras, which record simultaneously the front surface of the specimen during the tensile test. The relative position of the two cameras to each other and the position of the specimen in the 3D-space are assured by the calibration of the system. Hence, the out-of-plane movement of the specimen is corrected automatically and has no impact on the accuracy of the strain measurement. The full strain field on the front surface of the specimen is determined as a function of the longitudinal and transverse strains. Since the main focus of this investigation is on the volumetric behavior of the composites up to or only slightly beyond the yield point, the deformation monitored was completely homogeneous. In this case an average strain can be calculated by taking the mean of all sub-sets of the evaluated area, thus obtaining one average value for the longitudinal and the transverse strains, respectively. This averaging procedure increases the accuracy of the measurement significantly without any loss of information.

In addition to volume strain, the acoustic signals transmitted by the debonding of the particles were recorded for selected testing conditions and composites using a Sensophone AED 40/4 apparatus. Signals with amplitudes larger than 21 dB were recorded during the measurements. Volume strain and acoustic signals were recorded simultaneously on the same specimen to avoid errors coming from specimen-to-specimen variations.

2.3. Data reduction

The DIC system was applied in terms of technical strains to evaluate the essential data. True longitudinal strain $\varepsilon_{t,l}$ and true transverse strain $\varepsilon_{t,t}$ are given by

$$\varepsilon_{t,l} = \ln(1+\varepsilon_{n,l}) \tag{2}$$

and

$$\varepsilon_{t,t} = \ln(1+\varepsilon_{n,t}) \tag{3}$$

where $\varepsilon_{n,l}$ and $\varepsilon_{n,t}$ are the nominal longitudinal and nominal transverse strains, respectively. The Hencky strain definition enables us to calculate the volume strain ε_v by the combination of the three principal strains according to

$$\varepsilon_v = \varepsilon_{t,l} + 2\varepsilon_{t,t} \tag{4}$$

assuming that deformations are equal in the width and thickness of the specimen. Poisson's ratio, ν, was obtained in the strain range of 0.0005–0.0025 according to

$$\nu = -\frac{\varepsilon_{n,t2} - \varepsilon_{n,t1}}{\varepsilon_{n,l2} - \varepsilon_{n,l1}} \tag{5}$$

and the dilatational volume strain, $\varepsilon_{v,dil}$, is given by

$$\varepsilon_{v,dil} = \varepsilon_{t,l}(1-2\nu) \tag{6}$$

Nominal stress, σ_n, and true stress, σ_t, are defined as

$$\sigma_n = \frac{F}{A_0} \tag{7}$$

and

$$\sigma_t = \frac{F}{A_0(1-\varepsilon_{n,l}\nu_n)} = \frac{F}{A} \tag{8}$$

in which F is the force, A_0 the initial and A the actual cross-section of the specimen.

3. Results and discussion

3.1. Effect of particle size and content on deformation behavior

True strain vs. volume strain and true strain vs. true stress curves are presented in Fig. 1 for PP and PP-G3.5S at two different strain rates. As the strain rate decreases, lower stress levels are obtained both for the neat and the filled PP. The true strain–true stress curves are nonlinear from the very beginning of loading, thus no "kink" as suggested by Vollenberg et al. [4] can be detected on the curve and utilized for the determination of the onset of debonding. The volumetric response of neat PP in the strain range investigated can be roughly divided into three stages or components [20–25]. The first stage of increasing volume strain is caused by the negative hydrostatic pressure developing in tensile loading. The second stage developing on a local scale initially is related to the compaction of amorphous chains (involving local strain induced crystallization) and to the destruction of crystalline order accompanied and followed by various cavitation mechanisms (void formation, crazing and micro-cracking) in the third stage. While amorphous chain compaction results in a decrease of effective volume, the destruction of crystalline order and the appearance of the various cavitational mechanisms decrease the density and thus increase volume. In this stage of deformation (post-yield regime), cavitation is the dominating micromechanical deformation process, in which the increase in volume strain approaches the increase in longitudinal strain. Upon further strain significant shear-band formation may develop on a global scale under almost isochoric conditions and thus, volume strain levels off [26]. Finally, in the last stage of post-yield deformation (regime of strain hardening prior to ultimate failure) strain induced re-crystallization and post-crystallization also involving volume changes may take place on a global scale. The various competitive processes described depend on test conditions (strain rate and temperature).

Regarding the deformation range performed as part of the study, the first two stages described above are essentially responsible for volume strain changes up to the strain levels investigated (Fig. 1).

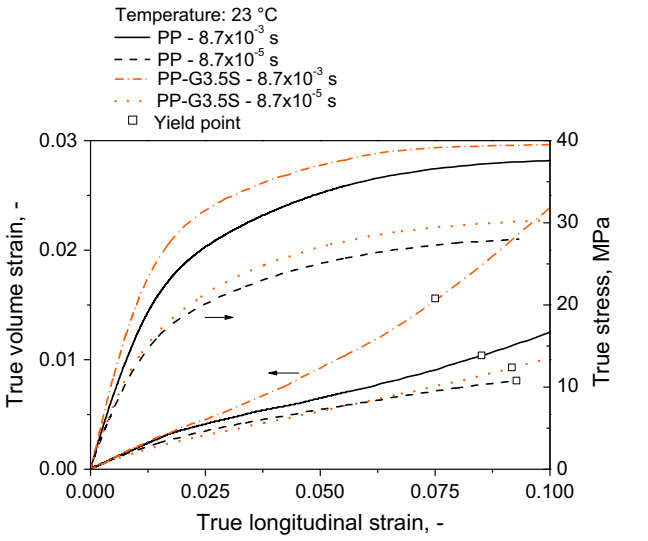

Fig. 1. True volume strain and true stress vs. true strain curves for PP and PP-3.5S recorded at two strain rates. The yield point was determined on nominal stress-strain curves.

The effect of hydrostatic pressure on van der Waals bonds is responsible for the increase of volume strain up to a longitudinal strain of about 0.020 for the materials investigated. In this range an almost linear relationship between true volume strain and true longitudinal strain was obtained, characterized by a constant Poisson's ratio. Upon further straining, the slope of the volume strain vs. longitudinal strain curve decreases significantly for the neat PP, which can mainly be attributed to the compaction of the amorphous phase [27]. When strain rate decreases, volume strain also decreases (i) as the applied stress decreases due to the visco-elastic nature of the material and so the hydrostatic pressure developed is smaller and (ii) the molecules have more time to get aligned in the direction of the load. In addition to the mechanisms described for neat PP, a relevant micro-deformation process in the composites is the debonding of the particles from the matrix, which considerably contribute to the volume strain increase. This can be observed when comparing the volume strain curves of PP and PP-G3.5S at the higher strain rate depicted (Fig. 1). The composite exhibits a significantly larger volume strain beyond 0.02 longitudinal strain, which can be directly related to the additional volume created by the detached particles. The difference between PP and the composite is remarkably reduced at the lower strain rate. Notably, the volume strain of PP-G3.5S is slightly smaller than that of PP at strains below 0.05 and almost identical values were determined for the two materials at the yield point. Void formation and crazing are typical deformation mechanisms in the neat PP before yielding of the specimen [26,28], which contributes to the volume increase. In the presence of particles, the stress fields change locally and thus may suppress cavitational deformation modes at least to some extent (as long as the matrix remains attached to the particles), and instead may initiate local shear yielding of the surrounding matrix [29].

The effect of particle size on the volumetric behavior is shown in Fig. 2 for the lowest strain rate of 8.7×10^{-5} s^{-1}. The comparison of the traces obtained for PP, PP-G3.5S and PP-G3.5L clearly shows that the volume strain of both composites is smaller up to a strain of 0.05. It is worth noting that this behavior is essentially explained by the suppression of cavitational deformation modes in the composite. However, the differences in the deformation of the matrix and composite are rather small and the volume strain–true strain traces of PP-G3.5L and PP-G3.5S coincide up to a strain of 0.03. Beyond this strain level the volume strain of PP-G3.5L is larger than that of PP-G3.5S, because of the lower debonding stress of larger particles as predicted by Eq. (1). This demonstrates that the behavior of composites in the linear regime in terms of, e.g., elastic modulus, Poisson's ratio and thermal expansion, is in general predominantly characterized by composite composition (i.e., filler content and properties) and not by nonlinear micro-deformations (e.g. debonding). Hence, the volume strain traces for the two composites PP-G3.5S and PP-G3.5L with the same composite composition are identical in the linear regime. According to the volume strain curves beyond the linear regime, particle debonding may initiate for the composite containing the larger glass beads and subsequently voids are created. The yield stress of PP-G3.5L is smaller than that of PP-G3.5S (Table 3), because of the smaller effective load-bearing cross-section of the specimen in the former case, which explains the strong dependence of the yield stress on particle size [30].

Table 3
Characteristic stress values of the studied composites determined at the strain rate of 8.7×10^{-3} s^{-1}.

Composite	Temperature, °C	Debonding stress, σ_D, MPa	Yield stress, σ_y, MPa	σ_D/σ_y, %
G3.5S	23	22.8	27.5	083
G3.5S	80	10.0	11.0	091
G7.0S	23	23.5	27.3	086
G7.0S	80	09.5	11.0	086
G3.5L	23	17.5	26.5	066
G3.5L	80	09.3	10.9	085
T3.5	23	26.4	27.9	095
T3.5	80	12.3	12.3	100
T7.0	23	27.0	28.7	094
T7.0	80	12.0	13.2	091

Volume strain depends on volume fraction of filler (composite composition), which becomes evident if we compare the traces of PP-G3.5S and PP-G7.0S. In the linear regime, volume strain increases mainly because of the different dilatational behavior of the composites. Adding glass beads to PP decreases Poisson's ratio and increases the dilatational volume strain (see Eq. (^)). In contrast to the small strain behavior, the volume strain–true strain curves in the yield and post-yield regimes may be attributed to the debonding of particles and micro-mechanisms of deformation (crazing and shear yielding). The slope in these curves at larger strains can be related to particle content [31,32], since the number and size of voids created are proportional to the volume fraction of the filler.

The effect of temperature on the deformation behavior of the various materials investigated is shown in Fig. 3, in which the traces of PP, PP-G3.5S, PP-G7.0S and PP-3.5L are compared. The volume

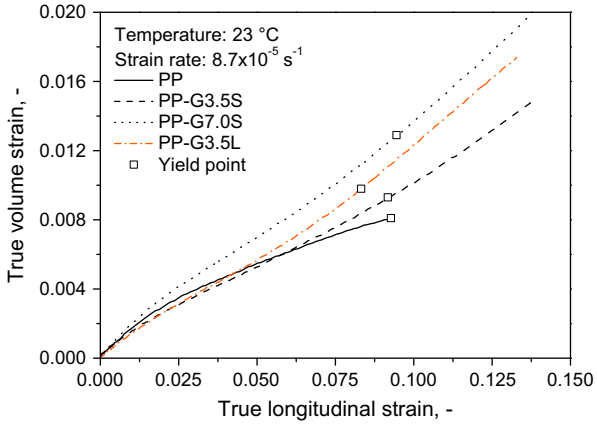

Fig. 2. Volume strain–longitudinal strain traces for neat and glass bead filled PP measured at 23 °C.

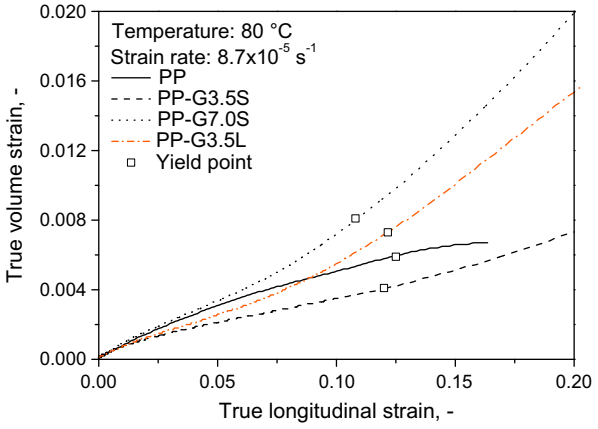

Fig. 3. Volume strain plotted as a function of longitudinal strain for PP and glass bead filled PP for a temperature of 80 °C.

strain of neat PP is smaller at elevated temperature than at 23 °C (see for comparison Fig. 6). The decrease of volume strain is mainly associated to (i) an increase of Poisson's ratio (close to 0.5 at 80 °C from 0.42 at 23 °C) and (ii) to the significant contribution of local deformations in the amorphous regime (amorphous chain compaction) [20]. While the composites containing the lower volume fraction of filler exhibit the same behavior in the linear regime, considerable differences were found in the nonlinear regime. It is worth noting that the two composites with the smaller volume fraction of filler have a significantly smaller volume expansion over a large strain range than the neat PP. This may be attributed to the suppression of dilatational micro-deformations in combination with debonding stresses approaching the composites yield stresses. According to Eq. (1), the debonding stress is proportional to the square root of the tensile modulus of the matrix. The yield stress decreases more significantly than the square root of the modulus, i.e., debonding takes place at stresses more closely to the yield stress at 80 °C than at 23 °C.

An increase in volume strain was detected for composites with the larger volume fraction of filler. Up to a strain of about 0.05, the shape of the volume strain–true strain curve is identical for PP-G7.0S and neat PP. Beyond this strain level the volume strain of the composite increases significantly due to the debonding process. Interestingly, such behavior can also be observed at the smaller volume fraction, but at larger strains (compare PP-G3.5S and PP-G7.0S). As the particle content increases, the local strain among the particles increases and various micro-deformation processes are initiated at smaller global strains.

3.2. Effect of particle shape and orientation on deformation behavior

True strain vs. volume strain and true strain vs. true stress curves are presented in Fig. 4 for PP and PP-T3.5 at two different strain rates. Due to the plate like particle geometry of talc, strain localization at the edges of these particles is significantly larger than for spherical particles. These high local strains lead to a noticeable reduction in the yield strain of the composite and to subsequent strain softening as a result of debonding. The characteristics of the true stress–true strain and true strain–volume strain traces changes significantly when platelets are added instead of spheres. Although the volume strain of PP-T3.5 is larger than that of the neat PP at the two strain rates, the difference decreases with decreasing strain rate. Minor differences were found in the volume strain of the two materials at yield, indicating that up to the yield point the dominating micro-mechanism of deformation is not debonding, but volume strain is determined by the effective volumetric behavior of the matrix. Beyond the yield point, the effect of strain rate on volume strain of PP-T3.5 is associated to the indirect dependence of the debonding stress on strain rate according to Eq. (1). The ratio of debonding stress to composite yield stress is larger for the slower loading speed than for the faster loading. In this context, debonding occurs to a lesser extent for the lower than for the higher strain rate, which is directly linked to the slope of the volume strain–true strain curve in the post-yield regime.

Volume strain–true strain curves measured at 80 °C are shown in Fig. 5 for PP and for composites with both talc contents. The behavior of the talc filled composites differs significantly from that of neat PP. At a strain value of about 0.01 the volume strain of the composites deviates from the one recorded for neat PP. Furthermore, the volume strain decreases in a strain range from 0.03 to 0.08 and starts to increase slightly before yield for the composite with the smaller filler content. Such a decrease in volume strain has also been observed for neat PE and PP by other authors and was related to volume compaction mechanisms (strain induced crystallization of amorphous regions) during tension loading [20,21]. However, in contrast, such a behavior was not detected for the neat PP in this study.

Nevertheless, the explanation that the reduction of volume strain may be associated with the compaction of amorphous chains in this specific strain range is supported by the prevailing local stress field in particulate filled composites. This behavior cannot be related to the interphase in particle filled composites [33–35]. The interphase consists of molecules attached to both the matrix and the particles, thus their mobility is significantly reduced. As a consequence, the transverse deformation during longitudinal straining is reduced leading to an effective decrease in Poisson's ratio. This in turn increases the volume strain of particulate filled composites but might not be the dominating micromechanical deformation process for the talc filled composite. Also in this context, debonding of particles is obviously not the dominating process up to the yield point for PP-T3.5. According to Eq. (1), the debonding stress is closer to the yield stress of the composite at 80 °C than at 23 °C. Hence, debonding may start beyond the macroscopic yield point and result in a significant increase of volume strain in the post-yield regime.

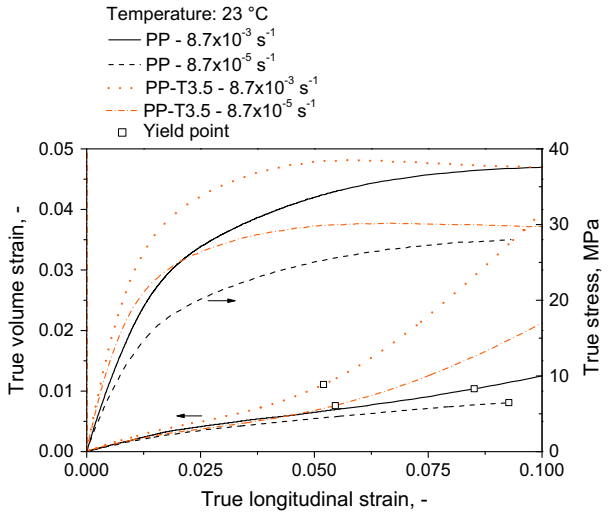

Fig. 4. True volume strain and true stress as a function of true longitudinal strain depicted for PP and talc filled PP.

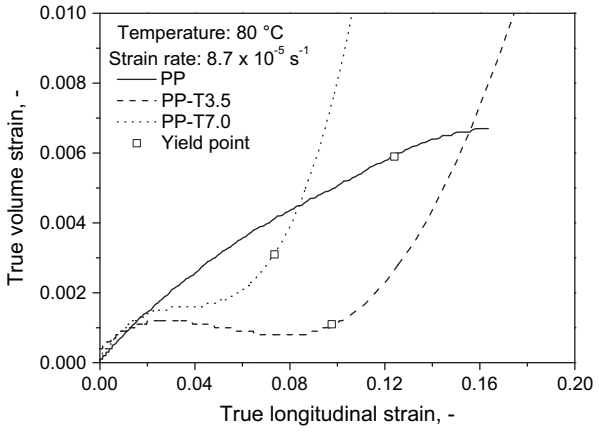

Fig. 5. Volume strain–longitudinal strain curves for neat PP and for composites containing different amounts of talc.

The volume strain curve of PP-T7.0 shows the same characteristic behavior as PP-T3.5. Strain localization between the particles increases significantly due to the larger volume fraction of filler and thus reduces the overall yield strain of the composite. Moreover, the prevailing level of local constraint also increases in the matrix, which may partly hinder amorphous chain compaction. It is worth noting that most of the particles are aligned in the direction of loading in the tensile specimen [36]. However, the orientation distribution of the particles also depends on particle content, as the space available for rotation in the melt flow process during specimen production is reduced with increasing filler content, but according to Pukánszky and Móczó [37] may not be significant and was therefore not considered in this work.

The influence of particle shape on volume strain behavior is compared in Fig. 6 for the composites with 3.5 v% filler content at 23 °C and 80 °C. Significant reduction of the volume strain can be observed with increasing testing temperature both for the neat PP and for the composites. While the dominating micromechanical deformation processes are apparently similar for the neat PP at both temperatures (similar shape of the volume strain–true strain curve) and the increased molecular mobility of the matrix results in the reduction of volume strain, the dominating deformation process changes significantly with temperature for the composites. This large change in behavior is caused by the difference in the ratio of debonding stress to yield stress at the two temperatures and by the increased molecular mobility of the matrix at 80 °C. The changing deformation mechanism may also explain the relative increase in the yield strain of PP-T3.5 compared to that of the neat PP as the temperature increases from 23 °C to 80 °C. The smaller volume strain of PP-T3.5 compared to that of PP-G3.5 may be attributed to the prevailing local stress field with higher shear stresses at the edges of the platelets in the talc filled composite [38]. The higher local stresses may initiate the local shear yielding of the matrix between two particles and suppress the cavitational modes of deformation. Since for PP-G3.5S no decrease of volume strain occurred in the strain range measured, amorphous chain compaction may not be of prime importance. On the other hand, in the talc filled composite a decrease in volume strain is clearly visible, indicating that amorphous chain compaction plays a role even outbalancing any destruction of crystalline order. The relative importance of chain compaction may be caused by increased crystallinity or thicker lamellae due to the nucleating effect of talc [39,40].

3.3. Determination of the debonding stress from volume strain measurements

In this section a new approach is introduced for the determination of debonding stress in polymer composites, which takes into account both the dilatational and the deviatoric behavior of the matrix and the composite. The volume strain of a polymeric can result from deviatoric, dilatational or cavitational deformation [9]. An appropriate approach has to account for the behavior of the matrix and for the difference in the dilatational response of the neat matrix and the composite because of the presence of the particles. Since in most cases stiff particles have a Poisson's ratio different from that of the matrix, the dilatation volume strain changes with particle content according to Eq. (6). Volume strain and dilatational volume strain are plotted as a function of true strain in Fig. 7. Dilatational deformation was detected for PP up to 0.02 true strain, while deviatoric deformation was observed subsequently up to 0.09 strain. Finally, cavitational mechanisms occur in the post-yield regime. In order to decouple the influence of the different dilatational behavior of the matrix and the corresponding composites, the dilatational volume strain is subtracted from the overall volume strain. The resulting curve represents volume change due to deviatoric and cavitational deformations (also including debonding of the particles) and is also depicted in Fig. 7. As in the selected example it may be negative, whenever the dilatational volume strain is larger in a certain strain range than the overall volume strain.

In order to subtract the deviatoric and cavitational volume strain of the matrix from that of the composite, a “corrected” true strain was calculated for the composites to account for the different global yield strains of the neat matrix and the composite, respectively. Since the local strain (and stress) is significantly larger in particle filled composites than in the neat matrix, yielding occurs at a smaller global strain. When comparing the yield strain of composites containing small and large glass beads, differences of the yield strain in the order of a few per cent caused by the dependence of debonding on glass bead size were obtained, which were neglected. Thus, to account for the different local strain states in the neat matrix and the composites and to obtain the “corrected” true strain value for a composite that corresponds to the true strain value of the neat matrix, the true strain of the composites was multiplied by the ratio of the matrix yield strain to the composite yield strain.

Subsequently the deviatoric and cavitational volume strain curves of the matrix were subtracted from that of the composite (true differential volume strain) using the “corrected” true strain.

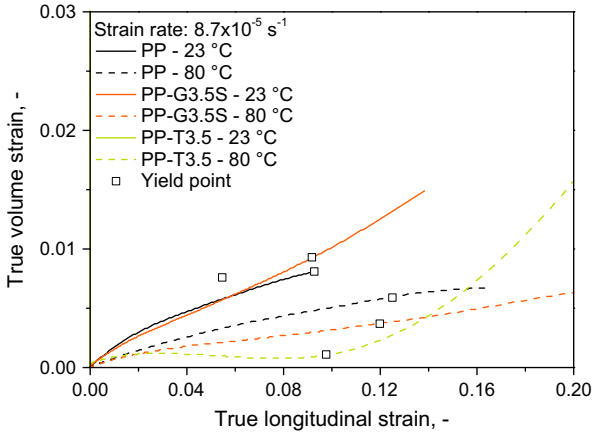

Fig. 6. Comparison of the volume strain traces for PP and PP composites at 23 °C and 80 °C.

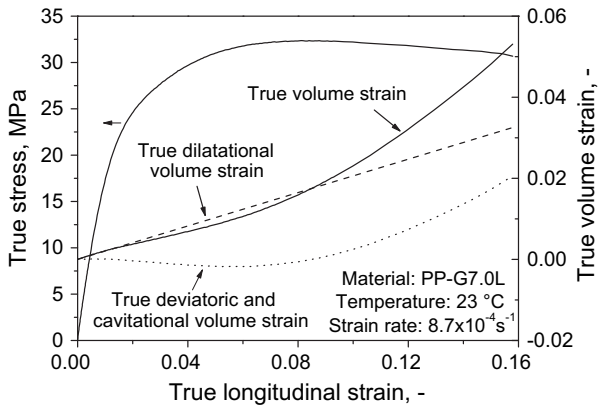

Fig. 7. Overall, dilatational, and deviatoric and cavitational volume strain plotted as a function of longitudinal strain; the stress-strain curve is also shown.

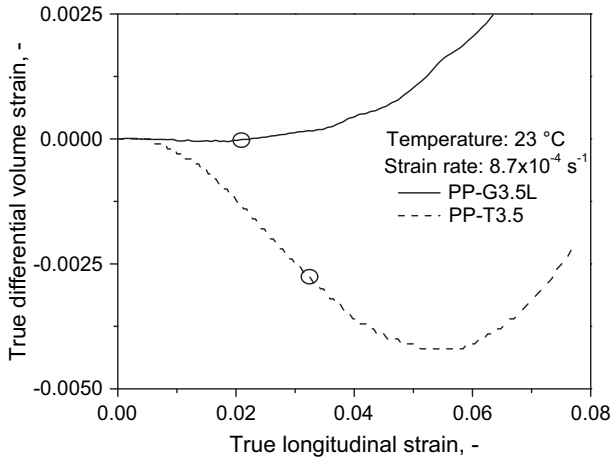

Fig. 8. True differential volume strain plotted as a function of true longitudinal strain for PP-G3.5L, which deforms with the same dominating micromechanical deformation mechanism as the neat PP, and for PP-T3.5 showing a significant change in the dominating micromechanical deformation. Circles indicate the onset of debonding.

The true differential volume strain vs. true strain traces are shown in Fig. 8 for PP-G3.5L and PP-T3.5. Note that Fig. 8 is plotted as a function of true strain and not against "corrected" true strain. The latter quantity was necessary only to subtract the deviatoric and cavitational volume strain of the matrix from that of the composite. For practical engineering reasons, the original global strain values were applied for the determination of the debonding stress.

Two principal cases can be distinguished when determining the onset of debonding.

- If the dominating micromechanical deformation process is the same in the matrix and the composite, the increase in the differential volume strain is related to debonding. This behavior was found for PP-G3.5L and is shown in Fig. 8, where the circle indicates the onset of debonding. The rate of debonding increases with increasing strain up to a certain strain level.
- A change in the dominating micro-mode of deformation may also result in a decrease of the differential volume strain (e.g., cavitational deformation modes in the matrix and shear yielding in the composite), as shown in Fig. 8 for PP-T3.5. In this case the onset of debonding was assigned to the point of inflection which was determined from the second derivative of the differential volume vs. longitudinal strain curve.

Utilizing the approach presented above, debonding stresses were calculated for the studied composites at different strain rates and temperatures. The effect of strain rate on the debonding stress is presented in Fig. 9 for the small and large glass bead composites as well as for talc composites. While the effect of strain rate on the debonding stress is not very pronounced (keeping in mind that only two orders of strain rate were investigated), the overall increase of the debonding stress with strain rate are in good agreement with theoretical predictions (Eq. (1)). Also evident from Fig. 9 is the effect of particle size on debonding stress, indicating that even small differences in particle size may considerably influence the performance of particulate filled composites. The largest debonding stresses were determined for the talc filled composites, which may be related to some extent to the large specific surface area of this filler. The results are summarized in Table 3 listing values for debonding and yield stresses and their ratio for the composites at two different temperatures and at the strain rate of $8.7 \times 10^{-5}\ s^{-1}$. As expected, the debonding stress is significantly closer to the yield stress at 80 °C than at 23 °C, irrespective of the filler type. For the talc filled composite, debonding stress and yield stress are approximately equal.

3.4. Acoustic emission

In order to validate the results obtained from the volume strain measurements, acoustic emission signals were detected during tensile loading. A true stress–true strain curve is presented in Fig. 10 for PP-G3.5L together with the individual acoustic signals detected during deformation. The majority of the events were detected in the pre-yield regime of deformation. The cumulative number of events was differentiated according to true strain and the maximum of the derivative function is considered as the strain, at which the rate of particle debonding is maximized [11,12]. A threshold amplitude of the signals was set to distinguish between background noise and particle-matrix interface failure. Also, small particles generate signals with significantly smaller amplitudes than large ones, which makes the identification of interfacial failure difficult. For the fillers investigated in this study, only the large glass beads provided a sufficient number of events during deformation. Despite several trials, no results of sufficient signal accuracy could be obtained when investigating composites containing the small glass beads and talc.

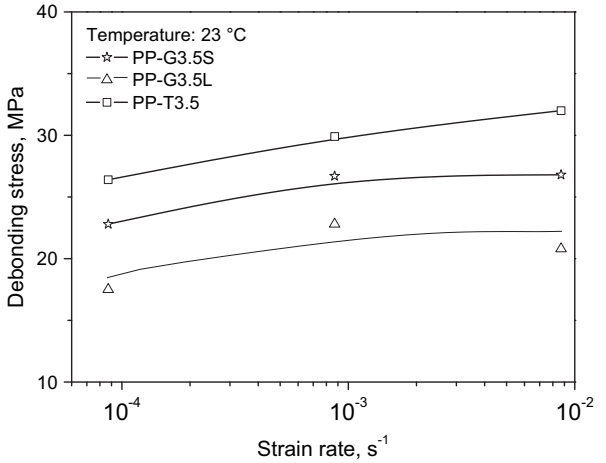

Fig. 9. Debonding stress plotted as a function of strain rate for the fillers studied.

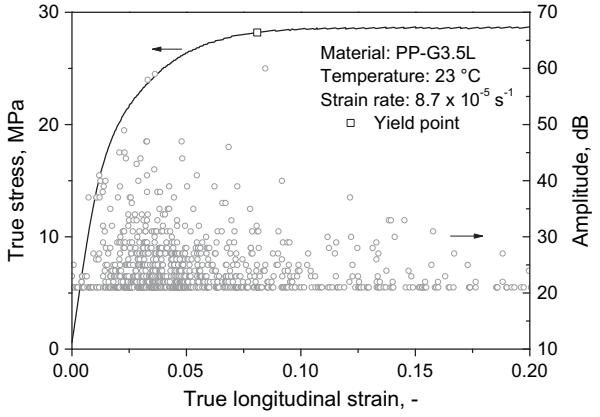

Fig. 10. True stress plotted against true strain together with the individual acoustic signals detected during the deformation of the sample.

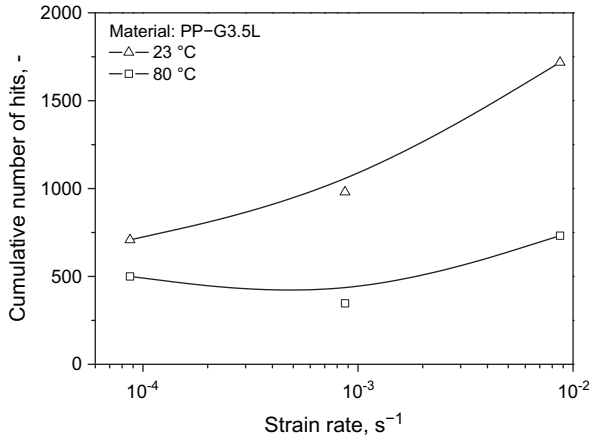

Fig. 11. Acoustic activity of PP-3.5L plotted against strain rate.

The cumulative number of acoustic events up to the yield stress is plotted as a function of strain rate for PP-G3.5L in Fig. 11. At 23 °C the number of signals increased significantly with increasing strain rate from 700 up to 1700. Simultaneously, the number of recorded events for 80 °C is significantly below the one for 23 °C, which is consistent with the results from volume strain measurements (i.e., debonding stress approaches the yield stress and fewer particles debond from the matrix at elevated temperatures). It should be mentioned, that the number of hits detected also depends on the damping behavior of the matrix. Thus, fewer signals were detected by the sensor with increasing temperature due to the associated damping increase and modulus decrease.

Debonding stresses determined by volume strain and acoustic emission measurements are plotted as a function of strain rate for PP-G3.5L in Fig. 12. The maximum in the derivative function of the cumulative number of hits was used for the determination of debonding stress by acoustic emission. Debonding stress values increase with increasing strain rate at both test temperatures (23 °C and 80 °C). Both methods acoustic emission and volume strain, yield significantly smaller debonding stress values at 80 °C than at 23 °C. At 23 °C the debonding stresses obtained by acoustic emission are about 20 % larger than those determined by volume strain measurements. Conversely, only insignificant differences were found at 80 °C, where at a strain rate of $8.7 \times 10^{-3}\,s^{-1}$ the debonding stress determined from volume strain was 9.3 MPa,

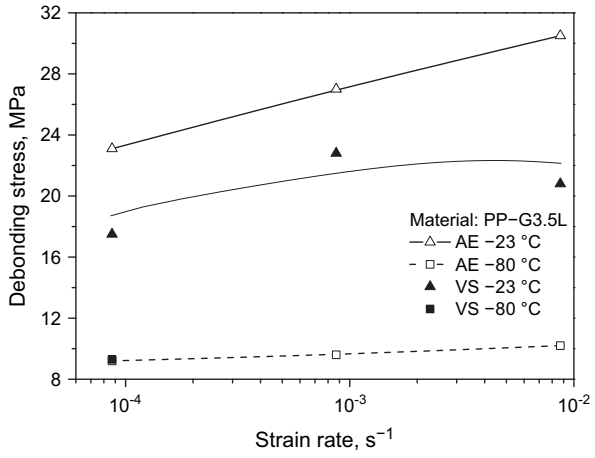

Fig. 12. Comparison of debonding stresses determined by acoustic emission and volume strain measurements at various strain rates.

while a value of 10.0 MPa was obtained by acoustic emission measurements. The larger debonding stresses at 23 °C derived from acoustic emission results may be related to the data evaluation procedure. As has been pointed out above, the data reduction procedure of the acoustic emission technique leads to a debonding stress at which the rate of debonding is maximized, while the volume strain technique yields the debonding stress values corresponding to the onset of debonding. For future studies, the peak value of the second derivative of the cumulative number of hits in acoustic emission measurements may provide a better estimate of the initiation of the debonding process and thus a more reliable number for the debonding stress.

4. Summary and conclusions

Tensile tests at two different temperatures (23 °C and 80 °C) in the strain rate range from $8.7 \times 10^{-5}\,s^{-1}$ to $8.7 \times 10^{-3}\,s^{-1}$ including volume strain measurements were carried out on PP containing glass beads of different size distributions and talc and on the neat PP used as matrix in the composite. The objective was to develop a methodology for the accurate characterization of the debonding process in these particulate filled composites and to determine the dominating micro-mechanisms of deformation. A significant increase in volume strain was recorded for composites containing the larger glass beads compared to those prepared with the smaller glass beads. The processes of local deformation in the matrix included various cavitational mechanisms (void formation, crazing and micro-cracking) and shear yielding, the majority being initiated prior to the yield point. The cavitational failure mechanisms (voiding, crazing, micro-cracking and debonding) were favored by the lower temperature (23 °C) and higher strain rates. At the elevated temperature (80 °C) or lower strain rates the volume strain of the composites was even smaller than that of the matrix, indicating a change in the dominating micro-mechanisms of deformation from the various cavitation mechanisms to local shear yielding. The volume strain of composites containing talc was also smaller than that of the neat PP. Volume strain decreased considerably in the pre-yield regime, indicating a complete change of the dominating micro-deformation process. The observed decrease in volume strain was explained by the compaction process of amorphous molecules and by the absence of debonding in this specific strain range. Based on the experimental results, a new approach was introduced for the determination of debonding stress values, which accounts for the dilatational behavior of the matrix and the composite, respectively, on the one hand, and for the deviatoric and cavitational deformation mechanisms of the matrix, on the other. The debonding stress was found to decrease with decreasing strain rate and increasing temperature, a result that agrees well with the prediction of theoretical models. Acoustic emission measurements were carried out to validate these results. Debonding stress values deduced from the latter experiments changed in the same way as a function of strain rate and temperature as the debonding stresses determined from volume strain measurements. However, the values determined by acoustic emission were somewhat larger, which was related to the data reduction procedure. Overall, the proper analysis of volume strain measurements in particulate filled composites provides useful information on the micro-mechanisms of deformation at various test conditions.

Acknowledgements

This research was performed at the Polymer Competence Center Leoben GmbH (PCCL, Austria) within the framework of the K_{plus}-program of the Austrian Ministry of Traffic, Innovation and Technology with contributions by the *University of Leoben,* and *Borealis*

Polyolefine GmbH. The PCCL is funded by the Austrian Government and the State Governments of Styria and Upper Austria. The research on heterogeneous polymer systems was partly financed by the National Scientific Research Fund of Hungary (OTKA Grant No. K 68748 and F 68579), we appreciate the support very much. One of the authors is indebted also to the János Bolyai Research Scholarship of the Hungarian Academy of Sciences.

References

[1] Markarian J. Plast. Addit Compd 2004;6:26.
[2] Morieras G. Ind Miner 2001;6:29.
[3] Pukánszky B. Particulate filled polypropylene: structure and properties. In: Karger-Kocsis J, editor. Polypropylene: structure, blends and composites, vol. 3. London: Chapman and Hall; 1995. p. 1.
[4] Vollenberg P, Heikens D, Ladan HCB. Polym Compos 1988;9:382.
[5] Vollenberg P. The mechanical behaviour of particle filled thermoplastics. PhD thesis, Eindhoven University of Technology, Eindhoven; 1987.
[6] Pukánszky B, Vörös G. Compos Interfaces 1993;1:411.
[7] Bai SL, Wang M, Zhao XF. Compos Interfaces 2003;10:243.
[8] Meddad A, Fisa BJ. Appl Polym Sci 1997;64:653.
[9] Naqui S, Robinson IM. J Mater Sci. 1993;28:1421.
[10] Yilmazer U, Farris RJ. Polym Compos 1983;4:1.
[11] Dányádi L, Renner K, Szabó Z, Nagy G, Móczó J, Pukánszky B. Polym Adv Technol 2007;17:967.
[12] Renner K, Henning S, Móczó J, Yang MS, Choi HJ, Pukánszky B. Polym Eng Sci 2007;45:1235.
[13] Pukánszky B, Van Es M, Maurer FHJ, Vörös G. J Mater Sci 1994;29:2350.
[14] Sinien L, Lin Y, Xiaoguang Z, Zongneng Q. J Mater Sci 1992;27:4633.
[15] Heikens D, Sjoerdsma SD, Coumans WJ. J Mater Sci 1981;16:429.
[16] Friedrich K. Adv Polym Sci 1983;52/53:226.
[17] Narisawa I, Ishikawa M. Adv Polym Sci 1990;91/92:354.
[18] Jerabek M, Ravi-Chandar K, Major Z, Lang RW. Mech Time-Depend Mater 2010;14:47.
[19] Jerabek M, Major Z, Lang RW. Polym Test 2010;29:407.
[20] Addiego F, Dahoun A, G'Sell C, Hiver JM. Oil Gas Sci Technol 2006;61:715.
[21] Addiego F, Dahoun A, G'Sell C, Hiver JM. Polymer 2006;47:4387.
[22] Na B, Lv RJ. Appl Polym Sci 2007;105:3274.
[23] Dasari A, Rohrmann J, Misra RDK. Mater Sci Eng A 2003;351:200.
[24] Kausch HH, Gensler R, Grein CH, Plummer CJG, Scaramuzzino P. J Macromol Sci 1999;38:803.
[25] Machado G, Denardin ELG, Kinast EJ, Goncalves MC, de Luca MA, Teixeira SR, et al. Eur Polym J 2005;41:129.
[26] Pawlak A, Galeski A. Macromolecules 2008;41:2839.
[27] Tang HI, Hiltner A, Baer E. Polym Eng Sci 1987;27:876.
[28] Oleinik EF. Polym Sci Ser C 2003;44:17.
[29] Dekkers MEJ, Heikens DJ. Appl Polym Sci 1985;30:2389.
[30] Fu SY, Feng XQ, Lauke B, Mai YW. Compos B Eng 2008;39:933.
[31] Farris RJ. Trans Soc Rheol 1968;12:315.
[32] Farris RJ, Falabella R, Tsai YD. ACS Symp Ser 1978;95:233.
[33] Pukánszky B. Eur Polym J 2005;41:645–62.
[34] Maurer FHJ, Kosfeld R, Uhlenbroich T, Bosveliev LG. Structure and properties of highly filled high-density polyethylene. In: 27th international symposium on macromolecules, Strasbourg, France, 6–9 July 1981.
[35] Kardos JL. In: Ishida H, Kumar G, editors. Molecular characterization of composite interfaces. New York: Springer; 1985. p. 1.
[36] Choi WJ, Kim SC. Polymer 2004;45:2393.
[37] Pukánszky B, Móczó J. Macromol Symp 2004;214:115.
[38] Herbst H. Modeling and simulation of the thermomechanical behavior of heterogeneous polypropylene compounds. Leoben: Montanuniversitaet Leoben; 2008.
[39] Ferrage E, Martin F, Boudet A, Petit S, Fourty G, Jouffret F, et al. J Mater Sci 2002;37:1561.
[40] Pukánszky B, Belina K, Rockenbauer A, Maurer FHJ. Composites 1994;25:205.